

Poisson's Ratios in Dynamic Viscoelasticity of Wood as Two-dimensional Materials.*¹

Nobuo SOBUE*² and Tomio TAKEMURA*²

木材の2次元動的粘弾性におけるポアソン比*¹

祖父江信夫*², 竹村富男*²

木材, 木質材料の2次元動的粘弾性挙動を数学的に表示するために, 一般化されたHookeの法則のアナロジーから, 平面応力下にある直交異方性粘弾性体の動的な応力-ひずみ関係式として(5)式を仮定し, 粘弾性定数 C_{IJ}^* と工学定数との関係を明らかにした((6)式)。この場合, 工学定数は複素数として(4)式で定義されるが, 特別な場合として弾性体の工学定数を含むものである。

つぎに, (4)式で定義される複素ポアソン比 ν_{YX}^* , ν_{XY}^* を実験的に求めるため, Fig. 2に示す装置を試作した。この装置を用いて測定したヒノキ, ブナ, ケヤキの ν_{YX}^* , ν_{XY}^* の絶対値および位相角の値を Table 2に示した。この結果から, 複素ポアソン比には位相にわずかの遅れがあり, また粘弾性定数 C_{IJ}^* は非対称なことが解った。

The present paper deals with mathematical expressions for the dynamic stress-strain relation of wood as two-dimensional anisotropic material, and the measuring of the complex Poisson's ratios.

A dynamic stress-strain relation in two-dimensions was assumed on the analogy of the generalized Hooke's law, and the relation between the elements of the tensor in Eq. 5 C_{IJ}^* and the complex "engineering constants" in Eq. 4 was investigated.

An electronic device was designed and used to measure the complex Poisson's ratios ν_{IJ}^* defined by Eq. 4 on Hinoki, Buna and Keyaki. The results are shown in Table 2. They suggest the existence of small delays in the phase angles of the complex Poisson's ratios, and also indicate asymmetric properties of the dynamic viscoelastic stiffness tensor C_{IJ}^* in Eq. 5.

1. INTRODUCTION

As developments of the advanced utilizations of wood and wood-based materials, the effective use of anisotropy of the materials has attracted many researchers in plywoods, laminated woods, L.V.L. and particleboards.

Plywoods and particleboards are often used as walls and floors. And their dynamic viscoelastic properties become important points in their utilizations, for instance, for sound-proofings and anti-vibration of floors by walking. Recently some parts of the sound boards of guitars and pianos were substituted by plywoods in place of solid

wood for the low cost of the plywoods. Wood and wood-based materials in these cases are apparently used as two-dimensional materials. But the progress in the dimensional generalization of the laws of dynamic viscoelasticity is fairly delayed comparing with that of elasticity.

One-dimensional theory of the dynamic viscoelasticity has almost been established. Then, an introduction of the concept of the Poisson's ratios to dynamic viscoelasticity will give a clue to the expansion of the one-dimensional law of dynamic viscoelasticity to two-dimensions as is analogized from the generalization of Hooke's law in elasticity.

In this paper, a formal generalization of Hooke's law to the dynamic constitutive equation of two-dimensional viscoelastic materials was investigated and the complex Poisson's ratios in the equation were also measured.

*¹Received October 4, 1978. Presented at the 27th Annual Meeting of the Japan Wood Research Society at Kyoto, April 1977.

*²名古屋大学農学部 Faculty of Agriculture, Nagoya University, Nagoya, 464 Japan.

2. COMPLEX POISSON'S RATIOS AND DYNAMIC CONSTITUTIVE EQUATION IN ORTHOTROPIC VISCOELASTIC BODIES

In this paper, a dynamic stress-strain relation of an orthotropic viscoelastic body was treated for the case of plane stress.

Denoting an axial cyclic stress applied in Y direction by σ_Y^* and the induced complex strains by ϵ_{YX}^* and ϵ_{YY}^* in X and Y directions respectively in Fig. 1, they may be expressed by the following complex exponential functions,

$$\left. \begin{aligned} \sigma_Y^* &= \sigma_Y e^{i\omega t}, \\ \epsilon_{YX}^* &= -\epsilon_{YX} e^{i(\omega t - \delta_{YX})}, \\ \epsilon_{YY}^* &= \epsilon_{YY} e^{i(\omega t - \delta_{YY})}, \end{aligned} \right\} (1)$$

where, t : time,

ω : angular velocity,

ϵ_{IJ}^* : complex strain component,

ϵ_{IJ} : amplitude of strain component ϵ_{IJ}^* ,

δ_{IJ} : phase angle.

In ϵ_{IJ}^* , ϵ_{IJ} and δ_{IJ} the first suffix denotes the direction of the applied stress and the second suffix the direction of the induced strain.

Similarly for an axial stress σ_X^* , the following strains arise,

$$\left. \begin{aligned} \epsilon_{XX}^* &= \epsilon_{XX} e^{i(\omega t - \delta_{XX})}, \\ \epsilon_{XY}^* &= -\epsilon_{XY} e^{i(\omega t - \delta_{XY})}, \end{aligned} \right\} (2)$$

and for a shearing stress τ_{XY}^* ,

$$\gamma_{XY}^* = \gamma_{XY} e^{i(\omega t - \delta_{SS})} \quad (3)$$

where γ_{XY}^* is a complex shearing strain.

The complex moduli of viscoelasticity corresponding to the so-called "engineering constants" in elastic bodies can be defined on the analogy of the case of an elastic body as follows:

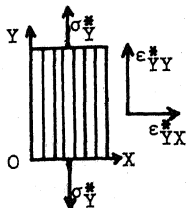


Fig. 1. Co-ordinate of an orthotropic plate, Y and X axes coincide with the principal axes.

$$\left. \begin{aligned} E_X^* &= \frac{\sigma_X^*}{\epsilon_{XX}^*} = \frac{\sigma_X}{\epsilon_{XX}} e^{i\delta_{XX}} = E_X' + iE_X'' \\ E_Y^* &= \frac{\sigma_Y^*}{\epsilon_{YY}^*} = \frac{\sigma_Y}{\epsilon_{YY}} e^{i\delta_{YY}} = E_Y' + iE_Y'' \\ G_{XY}^* &= \frac{\tau_{XY}^*}{\gamma_{XY}^*} = \frac{\tau_{XY}}{\gamma_{XY}} e^{i\delta_{SS}} = G_{XY}' + iG_{XY}'' \\ \nu_{XY}^* &= \frac{\epsilon_{XY}^*}{\epsilon_{XX}^*} = -\frac{\epsilon_{XY}}{\epsilon_{XX}} e^{i(\delta_{XX} - \delta_{XY})} = \nu_{XY}' + i\nu_{XY}'' \\ \nu_{YX}^* &= \frac{\epsilon_{YX}^*}{\epsilon_{YY}^*} = -\frac{\epsilon_{YX}}{\epsilon_{YY}} e^{i(\delta_{YY} - \delta_{YX})} = \nu_{YX}' + i\nu_{YX}'' \end{aligned} \right\} (4)$$

Here, attention should be paid to the point that the complex Poisson's ratio ν_{IJ}^* was also defined as a complex number.

A constitutive equation is one of the indispensable equations to characterize the stress-strain relation of the materials.

By assuming the small deformations in an orthotropic viscoelastic body, the dynamic stress-strain relations may be given after the generalized Hooke's law as follows:^{1),4)}

$$\begin{Bmatrix} \sigma_X^* \\ \sigma_Y^* \\ \tau_{XY}^* \end{Bmatrix} = \begin{bmatrix} C_{11}^* & C_{12}^* & 0 \\ C_{21}^* & C_{22}^* & 0 \\ 0 & 0 & C_{66}^* \end{bmatrix} \begin{Bmatrix} \epsilon_X^* \\ \epsilon_Y^* \\ \gamma_{XY}^* \end{Bmatrix} \quad (5)$$

This equation contains five constants corresponding to the so-called elastic stiffness in an elastic body, and the constants characterize the dynamic viscoelastic properties of an orthotropic material. We may call them "dynamic viscoelastic stiffness".

The dynamic complex moduli E_X^* , E_Y^* and G_{XY}^* are obtainable by putting $\begin{Bmatrix} \sigma_X^* \\ 0 \\ 0 \end{Bmatrix}$, $\begin{Bmatrix} 0 \\ \sigma_Y^* \\ 0 \end{Bmatrix}$ and $\begin{Bmatrix} 0 \\ 0 \\ \tau_{XY}^* \end{Bmatrix}$ into Eq. 5 respectively,

$$\left. \begin{aligned} E_X^* &= C_{11}^* (1 - \lambda^*), \\ E_Y^* &= C_{22}^* (1 - \lambda^*), \\ G_{XY}^* &= C_{66}^*, \\ \lambda^* &= \nu_{YX}^* \cdot \nu_{XY}^* = C_{12}^* C_{21}^* / C_{11}^* C_{22}^* \end{aligned} \right\} (6)$$

It is of interest to check the symmetry of the stiffness tensor in Eq. 5 in order to simplify the equation. The ratio of C_{12}^* to C_{21}^* is given by,

$$\frac{C_{12}^*}{C_{21}^*} = \frac{\nu_{YX}^* / \nu_{XY}^*}{E_Y^* / E_X^*} = \left| \frac{\nu_{YX}^*}{E_Y^*} / \frac{\nu_{XY}^*}{E_X^*} \right| e^{i(\delta_{XY} - \delta_{YX})} \quad (7)$$

If the coefficient of the exponential function in Eq. 7 is equal to unity as an elastic body, we can

write the ratio more briefly as follows:

$$\frac{C_{12}^*}{C_{21}^*} = e^{i(\delta_{XY} - \delta_{YX})} \tag{7'}$$

Of course, this relation may require an experimental verification.

3. EXPERIMENTS

3.1 Physical and dynamic viscoelastic properties of specimen used.

Species, specific gravities, moisture contents, sizes, dynamic Young's moduli and loss tangents of specimens are shown in Table 1.

The dynamic Young's moduli E' and the loss tangents $\tan \delta$ were measured by the method of free-free beam vibration. And E' was calculated from its resonance frequency, and $\tan \delta$ from the 0.707 value line width of the resonance curve.

3.2 Method for measuring complex Poisson's ratios.

In order to obtain the values of the complex Poisson's ratios in Eq. 4, the amplitudes ($\epsilon_{XY}/\epsilon_{XX}$, $\epsilon_{YX}/\epsilon_{YY}$) and the phase angles ($\delta_{XX} - \delta_{XY}$, $\delta_{YY} - \delta_{YX}$) from experiments are required.

One of the fundamental methods to measure these values is to draw a Lissajous' figure with a synchroscope. This method was used in this study.

The diagram of measuring devices used is shown in Fig. 2. A bar with rectangular cross-section is supported with strings at the two nodes of the lateral fundamental vibration. And a sinusoidal force is given by a magnetic driver at an end of

the bar in order to make the bar vibrate at its resonance frequency, which is measured by an inductance-type displacement meter and a universal counter at the end of the specimen.

The strains in longitudinal direction of the bar and in the perpendicular direction are measured by wire strain gages which are glued orthogonally to each other at the middle point of the bar.

The signals from the gages are amplified by strain amplifiers and transmitted to low-pass filters to remove the signals of the carriers at amplifiers, whose frequencies are 4kHz.

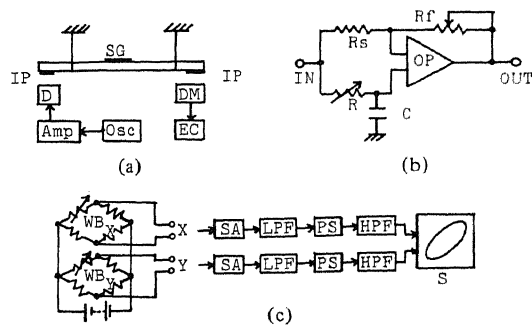


Fig. 2. Diagrams of measuring devices.

Driving system (a), Phase shifter^{2),3)} (b) and Electronic circuits system (c). Amp: Amplifier, EC: Electronic counter, D: Driver, DM: Displacement meter, HPF: High pass filter, IP: Iron piece, LPF: Low pass filter, OP: Operational amplifier, Osc: Oscillator, PS: Phase shifter, S: Synchroscope, SA: Strain amplifier, WB_x: WB_y: Wheatstone bridge.

Table 1. Physical and dynamic viscoelastic properties of specimens.

Species	Kind of vibration *1)	Moisture content (%)	Specific gravity	Dynamic Young's modulus ($\times 10^{10}$ dyne/cm ²)	Loss tangent	Sizes (cm)		
						Length	Breadth	Thickness
Hinoki <i>Chamaeciparis obtusa</i> Endl.	LR	12.1	0.40	5.80	0.008 ₆	35.1	5.04	1.20-1.24
	RL	12.5	0.41	1.22	0.018	28.1	4.52	1.50-1.63
Buna <i>Fagus crenata</i> Blume	LR	11.2	0.61	10.07	0.009 ₇	40.1	5.04	1.50-1.54
	RL	10.8	0.71	2.05	0.021	24.6	4.42	1.24-1.28
Keyaki <i>Zelkova serrata</i> Makino	LR	11.1	0.63	11.23	0.009 ₅	40.1	5.03	1.13-1.34
	RL	11.4	0.69	1.85	0.019	24.6	4.54	1.29-1.32

*1) The first letter denotes the longitudinal direction of the bar and the second letter the direction of the breadth of the bar. L; fiber direction of wood, R; radial direction of wood.

Numbers of the specimens used are three for each kind of vibration except LR specimens of Buna (two specimens).

Phase shifters are used to compensate the phase angles which are shifted by passing the amplifiers and other circuits.

High-pass filters are also used to remove the noises. Lastly the signals are transmitted to X and Y axes of a synchroscope and a Lissajous' figure is drawn.

The characteristics of the amplitude and the phase angle in electronic circuits depend on the frequency of signal, so that their adjustments are done as follows: A sinusoidal voltage whose frequency is equal to the resonance frequency of the sample is applied simultaneously to the out-put terminals of the Wheatstone bridge circuits WB_X and WB_Y , and the amplitudes and the phase angles are adjusted with the phase shifters looking at the Lissajous' figure in the synchroscope as shown in Fig. 3.

4. RESULTS AND DISCUSSIONS

Fig. 4 shows typical time-scanning figures of

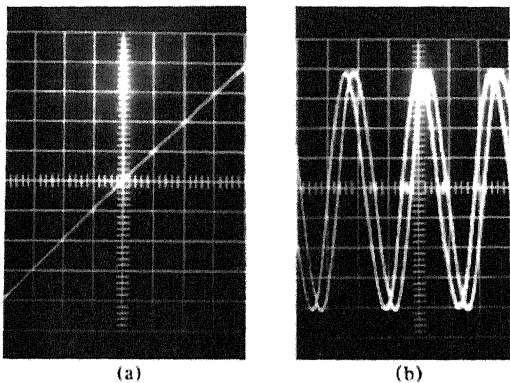


Fig. 3. Adjustments of the phase (a) and the amplitude (b) at the resonance frequency of a sample.

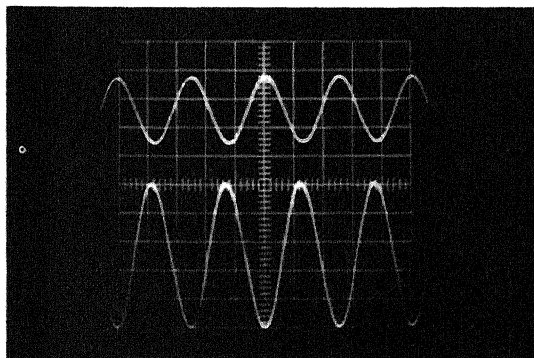


Fig. 4. Typical time-scanning figures of the dynamic strains at the resonance frequency.

the dynamic strains ϵ_{Y^*Y} and ϵ_{Y^*X} . The ratios of the double amplitudes, $|\epsilon_{Y^*X}|/|\epsilon_{Y^*Y}|$ and $|\epsilon_{X^*Y}|/|\epsilon_{X^*X}|$, are shown in Table 2 as $|\nu_{Y^*X}^*|$ and $|\nu_{X^*Y}^*|$ respectively.

Figs. 5 to 7 and Figs. 8 to 20 show the Lissajous' figures of the complex Poisson's ratios $\nu_{Y^*X}^*$ (the longitudinal direction of a specimen Y coincides with the fiber direction of wood) and $\nu_{X^*Y}^*$ (complimentary to $\nu_{Y^*X}^*$) respectively.

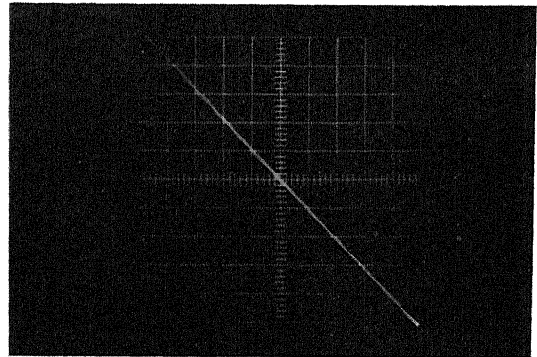


Fig. 5. Lissajous' figure of complex Poisson's ratio $\nu_{Y^*X}^*$ (Hinoki).

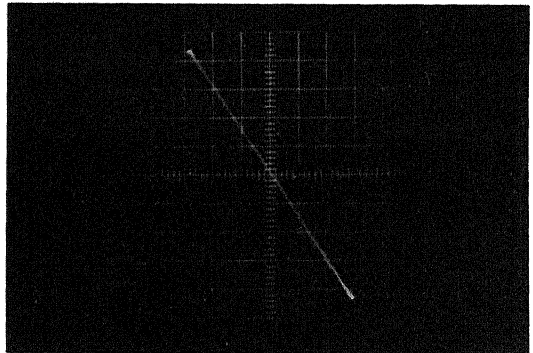


Fig. 6. Lissajous' figure of complex Poisson's ratio $\nu_{Y^*X}^*$ (Buna).

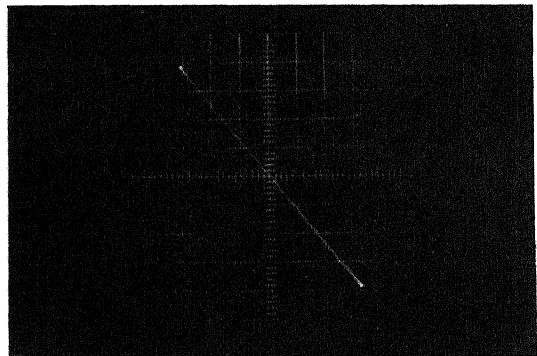


Fig. 7. Lissajous' figure of complex Poisson's ratio $\nu_{Y^*X}^*$ (Keyaki).

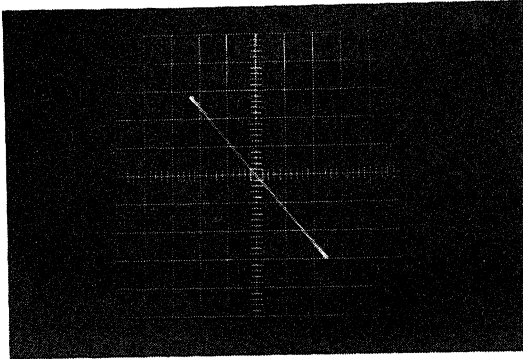


Fig. 8. Lissajous' figure of complex Poisson's ratio ν_{XY}^* (Hinoki).

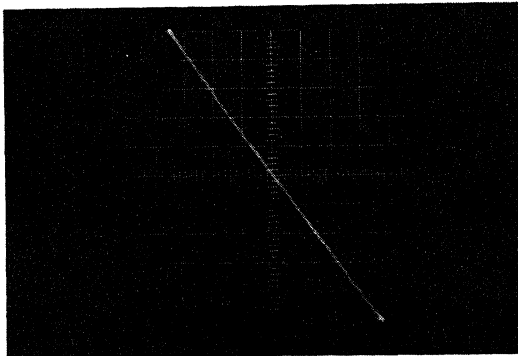


Fig. 9. Lissajous' figure of complex Poisson's ratio ν_{XY}^* (Buna).

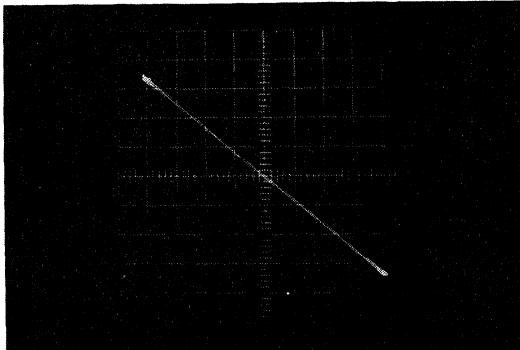


Fig. 10. Lissajous' figure of complex Poisson's ratio ν_{XY}^* (Keyaki).

As shown in Figs. 5 to 10, the loops of the Lissajous' figures of ν_{YX}^* and ν_{XY}^* were very narrow and the lines of the loops were overlapped. Then, the phase angles of ν_{YX}^* and ν_{XY}^* were calculated by the line breadth across the vertical axis in the synchroscope as shown in Fig. 11,

$$\sin \delta = \frac{b}{y} \tag{8}$$

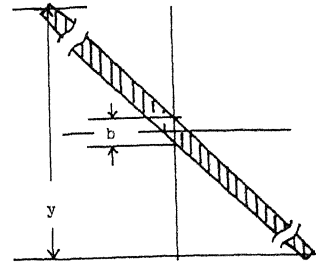


Fig. 11. Lissajous' figure and determination on phase angle δ .

$$\sin \delta = \frac{b}{y} .$$

The phase angles of ν_{YX}^* and ν_{XY}^* calculated by Eq. 8 are shown in Table 2. These values may be a little larger than the true values because they include the line breadth of a scanning beam which cannot be avoided in measurements. The corresponding angles of the line width of the scanning beam were from 0.021 to 0.032 rad. and 0.026 rad. in average.

The values of the phase angles of ν_{YX}^* and ν_{XY}^* in Table 2 are slightly larger than those calculated by the inherent beam width of the synchroscope used. This result suggests the existences of the delays in the phase angles of the complex Poisson's ratios, and the values in Table 2 are considered to give upper limits of the phase angles of the complex Poisson's ratios.

The interesting studies on the static Poisson's ratios by Schniewind⁵⁾ and Takemura⁶⁾ show the time-dependent changes of the Poisson's ratios in wood. Their results support the existences of the complex Poisson's ratios as is analogized from the theory of static viscoelasticity.

The measuring accuracy of the phase angles with a synchroscope or drawing the Lissajous' figures was not satisfactory in order to obtain the more definite values. Accordingly, another principle of the method to measure the phase angles should be contrived in future.

The conditions which give symmetry in the tensor in Eq. 5 are obtained from Eq. 7 as follows;

$$\left. \begin{aligned} \frac{|C_{12}^*|}{|C_{21}^*|} &= \frac{|\nu_{YX}^*|}{|E_Y^*|} \bigg/ \frac{|\nu_{XY}^*|}{|E_X^*|} = 1, \text{ and} \\ \delta_{XY} - \delta_{YX} &= 0 \end{aligned} \right\} \tag{9}$$

The values of the amplitude in Eq. 7 are shown in

Table 2. Complex Poisson's ratios ν_{YX}^* and ν_{XY}^* and absolute values of E_Y^* , E_X^* and C_{12}^*/C_{21}^{*1} .

Species	ν_{YX}^*		ν_{XY}^*		$ E_Y^* $ ($\times 10^{10}$ dyne/cm ²)	$ E_X^* $ ($\times 10^{10}$ dyne/cm ²)	$ C_{12}^* / C_{21}^* ^2$
	$ \nu_{YX}^* $	$\delta_{YY}-\delta_{YX}$ (rad.)	$ \nu_{XY}^* $	$\delta_{XX}-\delta_{XY}$ (rad.)			
Hinoki	0.43	-0.016	0.071	-0.037	5.85	1.24	1.28
Buna	0.32	-0.035	0.063	-0.040	10.17	2.09	1.05
Keyaki	0.40	-0.026	0.049	-0.039	11.34	1.89	1.36

1); mean values of 3 specimens except LR specimens of Buna (2 specimens).

2); See Eq. 7.

Y; fiber direction of wood, X; radial direction of wood.

Table 2 for three species. The fact that these values are not equal to unity indicates that the tensor in Eq. 5 is asymmetric. But, this result may not give a decisive complication to practical uses of the tensor, as we have experienced in cases of the treatment of cross stiffness of the static constitutive equations for wood and wood based materials.

5. CONCLUSIONS

As an attempt to extend the law of dynamic viscoelasticity from one-dimension to two-dimensions, it was presented to express the elastic stiffnesses as complex numbers on the analogy of the generalized Hooke's law. The dynamic constitutive equation given by Eq. 5 contains five independent dynamic viscoelastic constants C_{IJ}^* which are connected with five complex "engineering constants" E_X^* , E_Y^* , ν_{XY}^* , ν_{YX}^* and G_{XY}^* defined by Eq. 4, where the complex Poisson's ratios ν_{XY}^* and ν_{YX}^* are new constants defined in accordance with the introduction of anisotropy to the dynamic viscoelastic laws.

The values of ν_{YX}^* and ν_{XY}^* were obtained by the Lissajous' figures of cross strains with the devices shown in Fig. 2 and were shown in Table 2. The results suggested the existences of the delays in the phase angles of the complex Poisson's ratios.

And the values of the phase angles in Table 2 are considered as upper limits of complex Poisson's ratios for each species used.

Experimental results showed also that the dynamic viscoelastic stiffness tensor in Eq. 5 was asymmetric, being different from an elastic body.

By extending the law of dynamic viscoelasticity from one-dimension to two-dimensions, more detailed and systematic expressions for anisotropic dynamic behaviors are possible, and this will lead to the rational design of wood and wood-based materials as anisotropic materials.

REFERENCES

- 1) Love, A.E.H.: "A treatise on the mathematical theory of elasticity", 4th Ed., Dover Publications, New York, p. 97 (1952).
- 2) Tanaka, Y.: Audio & Electronics, 114, 185 (1976).
- 3) Ueno, T.: "Linear IC Handbook", CQ Publications, Tokyo, p. 122 (1973).
- 4) Hearmon, R.F.S.: "The Elasticity of Wood and Plywood", Forest Products Research, Special Report No. 7, London, p. 7 (1948).
- 5) Schniewind, A.P. and Barrett, J.D.: Wood Sci. and Tech., 6, 43 (1972).
- 6) Takemura, T.: Summary of Lecture of Rheology Symposium of Mokuzai Gakkai held at Nagoya in 1976, p. 7.